NANO LETTERS

LETTER

pubs.acs.org/NanoLett

# Effect of Growth Orientation and Diameter on the Elasticity of GaN Nanowires. A Combined in Situ TEM and Atomistic Modeling Investigation

Rodrigo A. Bernal,[†,⊥] Ravi Agrawal,[†,⊥] Bei Peng,[∥,†] Kristine A. Bertness,[‡] Norman A. Sanford,[‡] Albert V. Davydov,[§] and Horacio D. Espinosa[*,†]

[†]Department of Mechanical Engineering, Northwestern University, Evanston, Illinois 60208-3111, United States

[‡]Optoelectronics Division, National Institute of Standards and Technology, Boulder, Colorado 80305, United States

[§]Metallurgy Division, National Institute of Standards and Technology, Gaithersburg, Maryland 20899, United States

**ABSTRACT:** We characterized the elastic properties of GaN nanowires grown along different crystallographic orientations. In situ transmission electron microscopy tensile tests were conducted using a MEMS-based nanoscale testing system. Complementary atomistic simulations were performed using density functional theory and molecular dynamics. Our work establishes that elasticity size dependence is limited to nanowires with diameters smaller than 20 nm. For larger diameters, the elastic modulus converges to the bulk values of 300 GPa for *c*-axis and 267 GPa for *a*- and *m*-axis.

**KEYWORDS:** Gallium nitride nanowires, nanowire elastic modulus, in situ testing, first-principles calculations, molecular dynamics, size effect, surface reconstruction

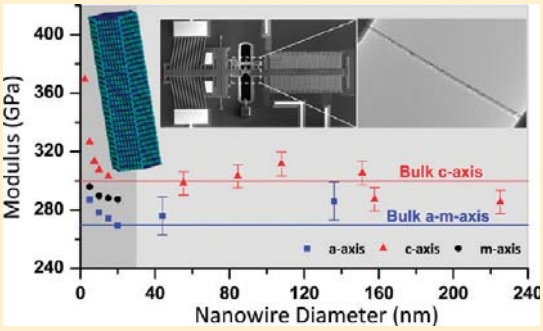


Gallium nitride (GaN) is a semiconducting material of current technological interest because of its various remarkable properties. This material has a tunable, direct bandgap, which makes it useful for optoelectronic applications such as lasers and light-emitting diodes (LEDs).[1,2] Its wide bandgap (3.42 eV)[1] also makes it ideal for power-electronics applications where high operational temperatures may be achieved.[3] Furthermore, GaN is known to be piezoelectric, which is relevant to the physics at the interfaces of semiconductor heterostructures used to create high mobility transistors,[4] and for energy-harvesting applications.[5]

In view of this unique combination of properties, GaN nanowires (NWs) have attracted great attention within the nanotechnology community because integration of its known functionality in nanosystems offers great potential for miniaturization and novel applications. For instance, transistors,[4] nanolasers,[6] nanoresonators,[7] and nanogenerators[8] have been demonstrated with single NWs of GaN or related compounds. The increasing interest in these nanomaterials underscores the importance of performing fundamental characterization of individual NWs.

Characterizing the mechanical properties of GaN NWs is essential to their application in nanodevices. For nanoelectromechanical systems in which deformation is required to achieve functionality, knowledge of the mechanical response of the individual building blocks is imperative. For example, to carry out an accurate analysis of devices that rely on their piezoelectric properties, such as nanogenerators,[8] a reliable estimation of the mechanical properties is required.[9] In the context of optoelectronic applications, mechanical characterization played an important role in the development of bulk GaN devices. Dislocations, caused by substrate−film lattice mismatch, often resulted in recombination traps that affected optical properties.[10] Mechanical characterization was used to evaluate films grown by techniques developed to overcome this problem.[11] In GaN nanowire growth, dislocations are rare;[10] however, mechanical properties may prove to be helpful in determining strains and stresses at the substrate−NW interface.

Earlier studies on the elastic modulus of GaN NWs span a range of techniques and methods. Experimentally, for *c*-axis NWs, the modulus was roughly estimated by resonance experiments in situ scanning electron microscope[7] (SEM). An atomic force microscopy (AFM)-based three point bending technique was used for the same orientation[12] and for *a*-axis NWs as well.[13] For *m*-axis NWs, electromechanical resonance in situ SEM[14] and transmission electron microscopy (TEM)[15] as well as nanoindentation experiments[16] were performed. Computational studies were also conducted to simulate buckling in the *c*-, *a*- and *m*-axis[17] and to predict the elastic response using a surface-energy model based on ab initio bulk-calculations (for *c*-axis NWs).[18] The elastic moduli reported in these studies are summarized in Figure 1.

Examination of the data clearly reveals large scatter in experimental and computational results. To put this in context, it is worth mentioning that precise identification of elastic constants has proven elusive even for bulk GaN.[1,19] However, compared to bulk measurements, the scatter for the reported values of Young's modulus of GaN NWs is much larger. This data scatter emphasizes the need for further studies to satisfactorily characterize the elastic properties of GaN NWs and also highlights the challenges

**Received:** September 30, 2010
**Published:** December 20, 2010

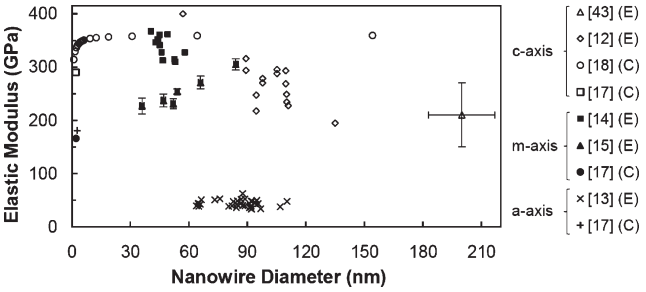


**Figure 1.** Plot of the experimental (E) and computational (C) results available in the literature for the elastic moduli of GaN NWs as a function of their diameter and axes (*c*-axis, open symbols; *a*-axis, solid symbols; *m*-axis, ticks). Note that data scatter is present in all orientations.

associated with nanoscale experimentation.[20] Such scatter and discrepancies in nanoscale experimentation and computation have also been reported for other materials.[21,22]

In this work, we focus on the elastic response of GaN NWs oriented along three different crystallographic axes of the wurtzite structure, namely, [0001] (*c*-axis), $[1\bar{2}10]$ (*a*-axis) and $[1\bar{1}00]$ (*m*-axis). We tackle the problem using a combined computational−experimental approach, as done previously for ZnO NWs.[23] We characterize experimentally *c*- and *a*-axis NWs using a MEMS-based in situ TEM uniaxial testing technique. Computationally, we model tensile tests on *a*-, *c*- and *m*-axis NWs using molecular dynamics with the Stillinger-Weber potential (SW-MD). For validation purposes, density functional theory calculations using generalized gradient approximation (DFT-GGA) were also performed on *c*-axis NWs. We demonstrate that there is no significant size dependence of elastic modulus for any growth axis, particularly in the size ranges that can be experimentally manipulated and tested, and that the deviation from bulk converges rapidly to the bulk values for wire diameters larger than 30 to 40 nm. We also show that differences in NW elastic modulus, for the studied growth orientations, are small, following the trend of bulk GaN.

The *c*-axis [0001]-oriented NWs used in this study were grown with molecular beam epitaxy (MBE) using a catalyst-free process that has been previously described.[24,25] In summary, the NWs are grown under conditions of high substrate temperature and high nitrogen pressure with no intentional doping, resulting in background carrier concentration around $10^{15}$ $cm^{-3}$. The growth orientation, using this method, is along the [0001] direction (*c*-axis) and sidewalls conform to the (six equivalent) $\{1\bar{1}00\}$ family of lattice planes (*m*-plane). However, the growth was such that the equivalent facets rarely displayed exactly the same area. The NWs are typically defect-free single crystals unless they merge during growth, and optical properties confirm their low background impurity concentration.[26] Unlike *c*-axis nanowires, the *a*-axis NWs were grown using the chemical vapor deposition (CVD) method, employing a direct reaction of gallium vapor with ammonia at 850−900 °C in a horizontal tube furnace.[27,28]

The NW samples were characterized prior to testing by high-resolution electron microscopy. Electron diffraction experiments in TEM confirmed that the dominant growth orientations of the samples were [0001] for the *c*-axis and $[1\bar{2}10]$for the *a*-axis in the wurtzite crystalline structure. The cross sections of the as-synthesized GaN NWs were examined using a field-emission SEM (FE-SEM). We observed hexagonal cross sections for *c*-axis NWs and triangular cross sections for *a*-axis (Figure 2). The facets are (i) $\{1\bar{1}00\}$for *c*-axis NWs[29] and (ii) $\{10\bar{1}1\}$ and {0001} for *a*-axis NWs.

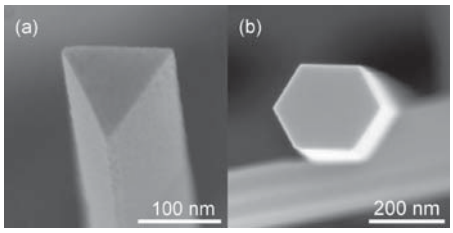


**Figure 2.** SEM images showing the typical cross sections of (a) *a*-axis GaN NW and (b) *c*-axis GaN NW.

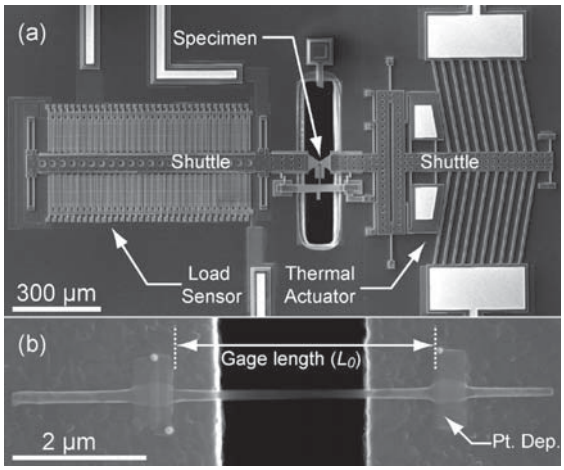


**Figure 3.** (a) SEM micrograph of the MEMS-based n-MTS. (b) Freestanding GaN NW suspended between actuator and sensor, welded by EBID of platinum.

The in situ TEM tensile tests were performed utilizing a MEMS-based nanoscale material testing system (n-MTS).[30−33] In this system, load is applied using a thermal actuator on one side of the freestanding specimen and is measured on the other side, using a differential capacitive load sensor based on interdigitated electrodes (see Figure 3a). The specimen is mounted between the actuator and load sensor shuttles (Figure 3b).

Mounting of the NW specimens onto the devices required their detachment from the growth-substrate. For the *c*-axis sample, this was achieved by ultrasonication of the growth-substrate in isopropyl alcohol, followed by dispersion of the resulting solution on top of a TEM grid.[23] For the *a*-axis sample, direct detachment of the NWs from the growth-matrix was performed. NWs were then chosen based on their diameter, picked either from the TEM grid or the growth-matrix, and mounted on the testing stage using a piezoelectric nanomanipulator.[23] The mounting process was performed inside a FE-SEM. The NW specimens were fixed to the testing stage by electron-beam induced deposition (EBID) of platinum (Pt) at both ends (Figure 3b). To avoid complications in the interpretation of data regarding the cross-sectional area, only nanowires with no noticeable taper in the gage region were tested.

After mounting, the specimens were tested in situ a high-resolution TEM (HRTEM). The testing methods and data reduction procedures to calculate the modulus of NWs in our experimental setup have been described previously.[23] Applied load, specimen deformation, and cross-sectional area are identified to compute the specimen's Young's modulus. Load was obtained by multiplying the load sensor's displacement by its


dx.doi.org/10.1021/nl103450e |*Nano Lett.* 2011, 11, 548–555

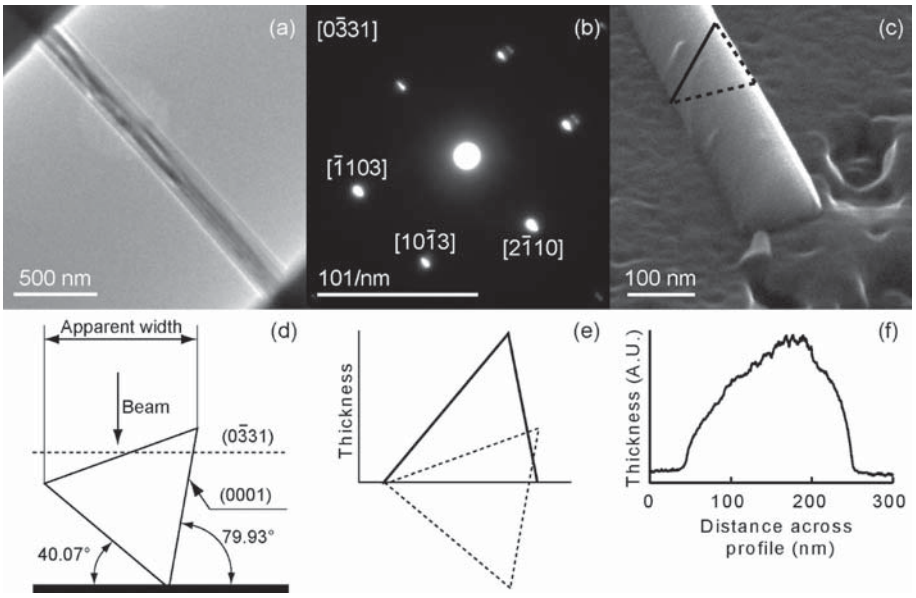


**Figure 4.** In situ TEM determination of a NW cross section, illustrated here for an *a*-axis nanowire. (a) View in TEM of the nanowire being tested. (b) Diffraction pattern of the NW with zone axis [0$\bar{3}$31]. (c) End of the *a*-axis NW lying on the testing device showing triangular cross section. (d) Knowing the cross-sectional shape, planes of the facets, and the zone axis, we can calculate the orientation of the NW with respect to the beam and the real dimensions based on the apparent width. (e) Expected thickness of the nanowire with the identified orientation. (f) Qualitative match of the expected thickness with an EELS thickness map. Note the asymmetry with respect to the center, which confirms an oblique angle of orientation with respect to the beam. The profile was obtained by integrating thousand line scans of a thickness-map image.

known stiffness;[32] the change in capacitance between the interdigitated electrodes of the load sensor was used to obtain the load sensor displacement.[30] The specimen's deformation was determined by digital image correlation of TEM images; specifically, the position of the shuttles was tracked across images of subsequent loading steps. The relative displacement of the shuttles is equal to the nanowire deformation, as there is no slippage in the EBID-Pt contacts.[23] Therefore, by dividing by the initial distance between the EBID-Pt contacts ($L_0$ in Figure 3b), the strain in the specimen was obtained.

The determination of cross-sectional area requires special attention, as it can lead to significant errors in the calculation of Young's modulus, particularly in polygonal-shaped specimens (such as hexagonal and triangular cross-section NWs), because only a projection of the real dimensions is seen in SEM or TEM images. As a result, a reliable method must be employed to estimate or directly measure the true NW cross sectional area. One approach reported in the literature is to assume a circular cross section and define the imaged NW width, which is a projection, as its diameter. Another approach sometimes used for hexagonal NWs is to assume that the observed width corresponds to two times the side of a regular hexagon. For hexagonal cross-section NWs, simple geometrical calculations suggest that the first approach (circular cross-section) can lead to overestimation of the cross-sectional area by up to 45%, while the second approach leads to up to 33% overestimation. Similarly, for triangular NWs, assuming the width is the base of an equilateral triangle, this can lead to overestimations as large as 25%. (Because of the crystal structure, triangular GaN nanowires are not exactly equilateral. However, the angles deviate less than 2° from 60°; therefore, this estimation was done assuming equilateral triangles.) The use of different assumptions regarding the cross-sectional area of NWs can explain in part the scatter observed in reported mechanical properties for GaN NWs. (A noteworthy exception is ref 15 where the specimens were rotated in TEM until maximum width was observed, which gives appropriate measurement of the cross-sectional area.)

In our experiments, the specimen cross-section was precisely measured either post-mortem in SEM or in situ TEM. If the specimen fractures, the cross section can be determined in SEM by direct observation of the fracture surface.[34] However, due to the limited stiffness of the testing system employed in some experiments, achieving fracture of NWs of large diameter was not always possible. In such cases, metrology performed in situ TEM was used to determine the cross-section.

TEM determination of the specimen cross section requires identification of the specimen's apparent width, orientation with respect to the beam, and shape of the cross section. The specimen's apparent width is directly measured from TEM images. TEM gives the advantage of accurately determining the edges of the specimen, as the crystalline lattice is differentiable from amorphous carbon or platinum, which can be deposited during in situ testing or specimen mounting. The specimen's orientation with respect to the beam is determined by obtaining a diffraction pattern and corresponding zone axis. Knowing the shape of the cross section, by observation of the ends of the specimen in SEM, and the crystalline plane of the NW's facets, the cross section can then be determined. Further qualitative confirmation of the specimen's orientation can be obtained by performing an electron energy loss spectroscopy (EELS) thickness map[35] and comparing it with the expected specimen thickness in the plane of the electron beam. The complete approach to obtain a NW cross-section by this method in situ TEM is illustrated in Figure 4. Note that this in situ approach lends itself better for specimens with high symmetry (such as triangular *a*-axis NWs). For *c*-axis NWs, given that the cross sections deviate slightly from regular-hexagonal, post-mortem observation of the fractured surface is preferred.


dx.doi.org/10.1021/nl103450e |*Nano Lett.* 2011, 11, 548–555

To complement the aforementioned experiments, atomistic simulations were performed. GaN NWs of different orientations and diameters were simulated using the open-source code LAMMPS.[36,37] The interatomic interactions were modeled using the modified Stillinger-Weber (SW) potential,[38,39] which is of the following form

$$E = \sum_i \sum_{j>i} \varphi_2(r_{ij}) + \sum_i \sum_{j\neq i} \sum_{k>j} \varphi_3(r_{ij}, r_{ik}, \theta_{ijk})$$

$$\varphi_2(r_{ij}) = A_{ij}\varepsilon_{ij}\left[B_{ij}\left(\frac{\sigma_{ij}}{r_{ij}}\right)^p - \left(\frac{\sigma_{ij}}{r_{ij}}\right)^q\right]\exp\left(\frac{\sigma_{ij}}{r_{ij} - \alpha_{ij}\sigma_{ij}}\right)$$

$$\varphi_3(r_{ij}, r_{ik}, \theta_{ijk}) = \lambda_{ijk}\varepsilon_{ijk}[\cos\theta_{ijk} - \cos\theta_{0ijk}]^2 \exp\left(\frac{\gamma_{ij}\sigma_{ij}}{r_{ij} - \alpha_{ij}\sigma_{ij}}\right)\exp\left(\frac{\gamma_{ik}\sigma_{ik}}{r_{ik} - \alpha_{ik}\sigma_{ik}}\right)$$

where $E$, the atomic energy, is composed of a two-body term $\varphi_2$ and a three-body term $\varphi_3$. Subscripts $i$, $j$, and $k$ represent the different atoms in the system. $\varepsilon_{ij}$ is the cohesive energy of the bond formed between atoms $i$ and $j$. $\alpha\sigma$ represents the cutoff distance. $\theta_{ijk}$ is the angle between $r_i$ and $r_k$ subtended at atom $j$ as vertex. Other terms, $A$, $B$, $p$, $q$, $\lambda$, and $\gamma$, are dimensionless fitting parameters adjusted to match the material properties. The values used in this study were taken from the work of Kioseoglou et al., which showed good agreement with the bulk elastic properties using these parameters.[38]

To validate the predictive capability of this semiempirical potential in the context of modeling the elastic response of GaN NWs, a comparative study was conducted against first-principles-based density functional theory (DFT) calculations. The SIESTA[40] software was used for DFT calculations with generalized gradient approximation (GGA) using Perdew−Burke−Ernzerhof (PBE) functional and double-ζ polarization (DZP) orbital basis sets. Pseudopotentials for all the atomic species were generated using the Troullier−Martins scheme[41] and were obtained from the SIESTA homepage.[42]

Simulations on bulk GaN were first conducted to ensure that lattice constants and elastic constants were being accurately predicted. Table 1 summarizes the lattice and elastic constants as predicted by DFT and SW calculations for bulk GaN, which are in reasonable agreement with each other, and with previously reported computational and experimental values (see Chapters 1 and 2 of ref 1 for a comprehensive review).

On the basis of the experimental observations of the cross sections, *c*-axis NWs were modeled with a hexagonal cross section, whereas *a*-axis NWs were modeled triangular. Despite that only triangular *a*-axis NWs were tested, some trapezoidal NWs were observed; thus, trapezoidal *a*-axis and *m*-axis nanowires were modeled as well (note that *m*-axis nanowires with trapezoidal cross-section have yet not been reported in the growth literature). Figure 5 shows the images of a *c*-axis-oriented hexagonal NW and *a*-axis-oriented NWs with different cross sections. For *a*-axis and *m*-axis NWs, two trapezoidal cross sections were modeled such that the distance, $h$, between two parallel {0001}-type planes (as shown in Figure 5c,d), was two-thirds and one-third of the total height $H$ of a triangular cross-section NW with the same diameter $D$. Note here our definitions of diameter, which apply for experimental and computational results. For a hexagonal NW, the diameter is defined as its major axis; for a triangular NW, it is defined as the width of its (0001) facet.

To compute the elastic modulus of NWs, the total energy ($E_{\text{total}}$) of the NW system was plotted as a function of axial strain ($\varepsilon$). A second order polynomial was fitted in the elastic regime with $\varepsilon < 2\%$. The second derivative of this polynomial was then used to compute the elastic modulus, $Y$, as

$$Y = \frac{1}{V_0}\left(\frac{\partial^2 E_{\text{total}}}{\partial \varepsilon^2}\right)_{\varepsilon = 0}$$

where $V_0$ is the initial NW volume at equilibrium.

We investigated size effects on the elastic modulus of *c*-, *m*- and *a*-axis GaN NWs with the experimental and computational methods described above. For *c*-axis, we simulated NWs with diameter ranging from 2.4 to 15 nm and experimentally tested NWs with diameter in the range of 55 to 225 nm. For *a*-axis NWs, simulations were performed for diameters ranging from 5 to 20 nm, and two experiments were conducted on NWs with diameters 44 and 136 nm. For *m*-axis NWs, given the good agreement between experiments and simulation for the previous cases, only simulations were performed. Here the NW diameters ranged from 5 to 20 nm.

For *c*-axis NWs, DFT and MD simulations and experiments reveal a consistent trend for the dependence of elastic modulus on diameter, as shown in Figure 6. Simulations on a 2.4 nm

**Table 1. Bulk Properties for GAN As Calculated Using DFT-GGA and SW Potential**

| | $c$ (Å) | $a$ (Å) | $c/a$ | $c_{33}$ (GPa) | $c_{11}$ (GPa) |
|---|---|---|---|---|---|
| DFT -GGA | 5.246 | 3.283 | 1.597 | 361 | |
| SW | 5.165 | 3.231 | 1.598 | 384 | 378 |

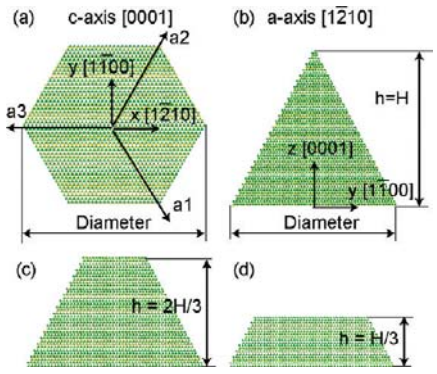


**Figure 5.** Cross-sectional views of GaN NWs models: (a) *c*-axis; (b) triangular *a*-axis; (c,d) trapezoidal *a*-axis with $h = 2H/3$ and $h = H/3$.


dx.doi.org/10.1021/nl103450e |*Nano Lett.* 2011, 11, 548–555

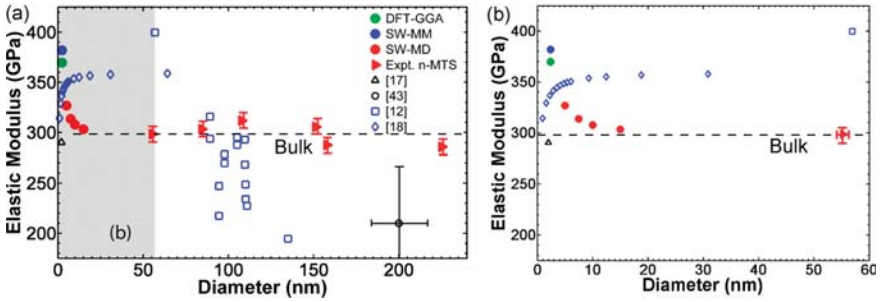


**Figure 6.** (a) Consolidated results for modulus of *c*-axis GaN NWs as a function of diameter. The results from this work are plotted in filled symbols. The dashed line represents the bulk value as predicted by SW potential; (b) zoom-in of image (a) in the diameter range of 0 to 60 nm, showing that the size effect disappears within NWs 20 nm in diameter.

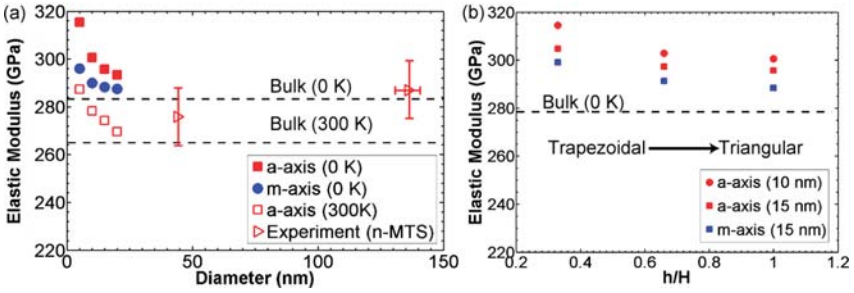


**Figure 7.** (a) Elastic modulus as a function of wire diameter for triangular *a*- and *m*-axis NWs; (b) effect of cross-section (triangular vs trapezoidal) on *a*- and *m*-axis NWs.

diameter NW, conducted with DFT-GGA and SW-MM, predicted values of 369.6 and 381.9 GPa, respectively, which are in agreement within 4% and are consistently higher than the bulk value of 300 GPa. These results validated the use of SW potential for characterizing the elastic response of GaN NWs. Further simulations, using SW-MD at 300 K, on NWs with diameter ranging from 5 to 15 nm, predicted size effects where the elastic modulus decreased as the NW diameter increased. The elastic modulus was predicted to converge to the bulk value for a diameter larger than 20 nm, and therefore, no size-dependence was anticipated in the experimentally tested regime. Indeed, the experiments revealed an average modulus of 304 ± 8 GPa independently of nanowire diameter. Measurements were performed on five NW specimens, all of which were larger than 50 nm in diameter.

Figure 6 summarizes the combined experimental−computational results obtained for *c*-axis NWs in this investigation. The figure also provides a comparison between results reported here and other values reported in the literature. Note that our results reveal a consistent trend and a narrower band in the experimental values. Our findings differ from the results reported by Chen et al.,[12] Brown et al.,[43] and Gulans and Tale[18] but are in agreement with the estimation performed by Tanner et al.[7] The results from Chen et al., as such, show no consistent modulus size-dependent trend, but rather a very large scatter in measured modulus, primarily below 300 GPa. This is likely due to the nonrepeatable and not well-defined boundary conditions in their experiments, as they had to use the fixed−fixed or simply supported models interchangeably to fit their three-point AFM bending data.[12] The differences between the measurements here reported and those reported by Brown et al.[43] may be explained by their assumption of circular cross-section, diameter determination in SEM (which may lead to overestimations), accuracy in load measurement, and slippage in the nanowire clamps. On the computational side, the results from Gulans and Tale are based on first principles calculations. However, they did not simulate actual NWs of various diameters. Instead, they looked at the energy differences arising from the surfaces expected in NW facets.[18] Although this can potentially capture the contribution of the surface to the elastic modulus' size-dependence, it misses the actual interaction between the surface and the core of the NW, which plays a significant role. As a result, a trend opposite to the one identified in this work was obtained. The result from Wang et al.[17] is also plotted in Figure 6 but we do not discuss it because only one case was simulated in their study. However, we note that the reported modulus is smaller than the Young's modulus identified for bulk, in direct contrast to the values obtained in our simulations.

For *a*- and *m*-axis NWs, similar size dependence was observed, that is, the modulus decreased as the NW diameter increased (as shown in Figure 7a). Once again, the size effects were observed to be prominent only for NWs with diameters smaller than 20 nm. For *a*-axis, the experimental results yielded moduli of 276 ± 13 GPa for the 44 nm diameter NW and 286 ± 13 GPa for the 136 nm NW, which agrees well with the bulk prediction of 266.7 GPa at 300 K. Note that the 136 nm nanowire had a grain boundary, running parallel to the growth axis (or uniaxial-tensile direction) along all the gage length.[44] For *a*- and *m*-axis, our results differ from previously measured values. However, note that the study of Henry et al.[14] covered a narrow range of nanowire diameters, and therefore the measurements can be considered as representative of the scatter of their experimental technique (in situ SEM resonance). The study of Nam et al.[15] shows a size-dependence of the modulus with a more pronounced trend (smaller diameters lead to smaller modulus, see Figure 1). Both these studies are based on mechanical resonance that may have a greater contribution of surface elasticity arising


dx.doi.org/10.1021/nl103450e |*Nano Lett.* 2011, 11, 548–555

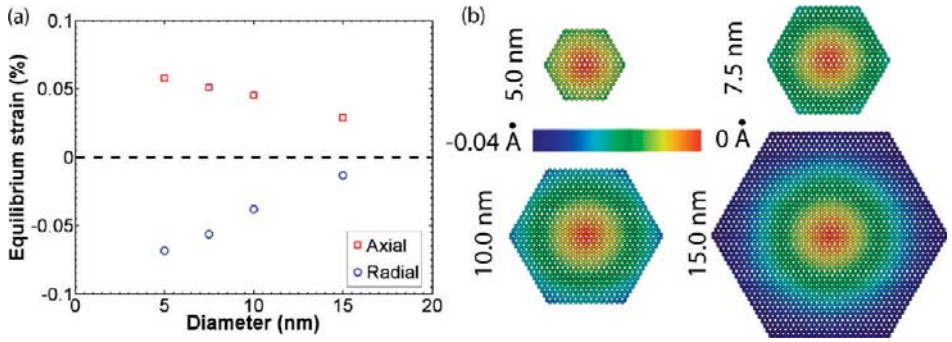


**Figure 8.** (a) Equilibrium strains obtained for *c*-axis NWs of different diameters after initial relaxation; (b) radial displacements in the cross-section.

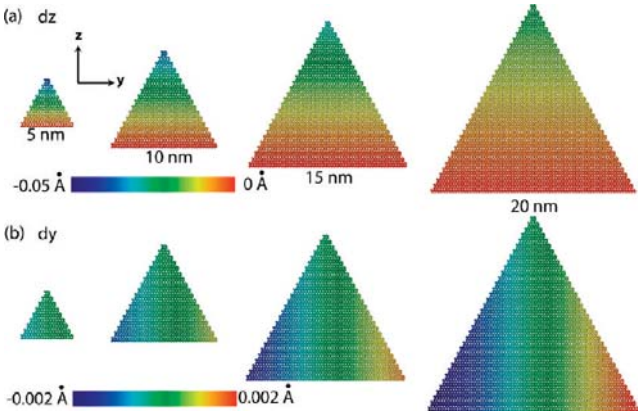


**Figure 9.** Displacements in *z*- (a) and *y*- (b) directions in the cross-section of *a*-axis NWs for different diameters.

from flexural deformation.[45] Additionally, the apparent measured elastic modulus via resonance in an electric field depends on the applied fields and the aspect ratio of the specimen,[46] which might have affected the results if both these parameters were not controlled.

For these nonpolar orientations, we also analyzed the effect of cross-sectional geometry. Figure 7b shows the modulus for different NWs cross sections. It was observed that trapezoidal NWs have 15−20 GPa higher modulus as compared to triangular NWs of the same diameter.

It is important to point out that the size-dependent trends observed in these simulations are highly unlikely to be captured in the experiments due to the following reasons: (i) it is quite challenging to manipulate and test NWs smaller than 20 nm in diameter; (ii) the experimental error can range from 15 to 30 GPa (for this material), which is of the same order of magnitude as the variation predicted by the simulations.

To understand the origin of the size-dependence of the modulus, we analyzed the atomic structure after initial minimization of the atomistic models. The objective was to observe the effect of surface atoms and how their reconstruction affects the overall initial atomic structure of the NW. In general, it was found that in all cases (irrespective of the axes) there was an effective reduction in the cross-sectional area. For *c*-axis NWs, slight expansion along their axis was also observed (as shown in Figure 8a). However, the radial contraction (Figure 8b) due to surface relaxation seems to be the prominent contribution to the reduction of the interatomic spacing. The mechanism leading to the size effect is, therefore, similar to what was observed in ZnO.[23] The effective reduction of interatomic spacing leads to increased stiffness, as the elastic modulus $E$ scales with $d^{-4}$ with $d$ being the interatomic spacing.[23,47] However, we note the following differences between the behavior of ZnO and GaN: (i) the relaxation strains (both axial and radial) are smaller for GaN and (ii) the radial contraction for GaN is uniform, and no localized effect on the surface is observed. For *a*- and *m*-axis GaN NWs, a lateral contraction was observed along the *z*-axis (as shown in Figure 9a), similar to *c*-axis NWs. However, there was no axial elongation corresponding to this contraction for these axes, instead there was a minor expansion (smaller by an order of magnitude) observed along the transverse *y*-axis (Figure 9b). Hence, the size effect arises from overall contraction along the cross-section, leading to reduced interatomic spacing and higher modulus for smaller NWs.

It is worth mentioning that zinc oxide (ZnO) NWs, oriented along the *c*-axis with the same type of crystal structure, exhibit a more pronounced elasticity size effect than GaN. In ZnO, the modulus of a 5 nm NW is 40% higher than bulk[23] as compared to a mere 10% increase seen in GaN for the same diameter. This difference in moduli between the two materials suggests that the deviation from the bulk atomic configuration is larger in the case of ZnO nanowires, which is also apparent from the equilibrium axial and radial strains observed for the two materials after energy minimization. Equilibrium axial strains observed in the case of ZnO NWs are almost 5 times larger than those in GaN, which suggests that surface stresses are more prominent in ZnO. Furthermore, we believe that the lower bulk modulus of ZnO also leads to a more pronounced elasticity size effect in this material, as its structure is relatively more prone to be deformed by relaxation-induced surface stresses. Following this hypothesis, one may generalize that a wurtzite compound with lower elastic modulus will display a more pronounced elasticity size-effect and vice versa.

As a conclusion, we can say that GaN NWs greater than 20 nm exhibit bulk properties. The reason for this is the high stiffness of GaN, which inhibits significant surface reconstruction. Furthermore, there is not a pronounced anisotropy between the different growth axes, just as in bulk GaN.[16] Therefore, in terms of elastic modulus, there appears to be no particular advantage in using a specific axis in GaN NW nanosystems.

In summary, we have presented a computational−experimental investigation to identify the elastic modulus of GaN NWs for three major growth orientations, namely the *c*-, *a*- and *m*-axes. Our computational results indicate that bulk behavior for all the axes is attained as the NW characteristic dimension increases beyond 20 nm. This fact was confirmed by experimental results


dx.doi.org/10.1021/nl103450e |*Nano Lett.* 2011, 11, 548–555

performed on *c*- and *a*-axis NWs with diameters larger than 40 nm, which exhibited bulk behavior. In our experiments, TEM observation allowed for accurate metrology of the cross-sectional area avoiding artifacts that may be present in observation by SEM or other methods. Finally, we assert that NWs attain bulk behavior at very small scales. In view of the fact that GaN bulk crystal does not exhibit pronounced anisotropy, there is no advantage of selecting one axis orientation over the others in terms of elastic properties. Our findings present a consistent picture, from very small sizes up to hundreds of nanometers, which compare well with previous studies for bulk behavior. As such, the study provides conclusive findings on the mechanical properties of GaN NWs. In this regard, the results here reported can be used with confidence in investigations in which mechanical behavior of GaN NWs is exploited.

## AUTHOR INFORMATION


### Corresponding Author

*E-mail: espinosa@northwestern.edu. Phone: (847) 467-5989. Fax: (847) 491-3915.

### Present Addresses

[||]Department of Mechanical Engineering, University of Electronic Science and Technology of China, 2006 Xiyuan Road, Chengdu, China.

### Author Contributions

[⊥]These authors contributed equally to this work.


## ACKNOWLEDGMENT

This work was supported by the National Science Foundation under Awards Number DMR-0907196, CMMI-0555734, and EEC-0647560. We thank Dr. Abhishek Motayed from University of Maryland for providing *a*-axis GaN nanowires for mechanical testing. We thank I. Petrov and E. Olson for their contribution in the development of the in situ TEM holder. We thank Dr. Shuyou Li and Dr. Tobin Filleter for assistance during TEM testing. We also acknowledge Dr. Michael Baskes from Los Alamos National Laboratories and Dr. S. G. Srivilliputhur from University of North Texas for insightful discussions concerning the atomistic models.

## REFERENCES


(1) Morkoç, H. *Handbook of Nitride Semiconductors and devices*; Wiley-VCH Verlag GmbH & Co.: Weinheim, 2008; Vol. 1.

(2) Nakamura, S.; Pearton, S.; Fasol, G. *The Blue Laser Diode: The Complete Story*. Second ed.; Springer-Verlag: Berlin, 2000.

(3) Yao, T.; Hong, S.-K. *Oxide and Nitride Semiconductors: Processing, Properties and Applications*; Springer-Verlag: Berlin, 2009; Vol. 12.

(4) Li, Y.; Xiang, J.; Qian, F.; Gradeĉak, S.; Wu, Y.; Yan, H.; Blom, D. A.; Lieber, C. M. Dopant-Free GaN/AlN/AlGaN Radial Nanowire Heterostructures as High Electron Mobility Transistors. *Nano Lett.* **2006,** *6* (7), 1468–1473.

(5) Wang, Z. L. Towards Self-Powered Nanosystems: From Nanogenerators to Nanopiezotronics. *Adv. Funct. Mater.* **2008,** *18* (22), 3553–3567.

(6) Johnson, J. C.; Choi, H.-J.; Knutsen, K. P.; Schaller, R. D.; Yang, P.; Saykally, R. J. Single gallium nitride nanowire lasers. *Nat. Mater.* **2002,** *1* (2), 106–110.

(7) Tanner, S. M.; Gray, J. M.; Rogers, C. T.; Bertness, K. A.; Sanford, N. A. High-Q GaN nanowire resonators and oscillators. *Appl. Phys. Lett.* **2007,** *91* (20), No. 203117-3.

(8) Huang, C.-T.; Song, J.; Lee, W.-F.; Ding, Y.; Gao, Z.; Hao, Y.; Chen, L.-J.; Wang, Z. L. GaN Nanowire Arrays for High-Output Nanogenerators. *J. Am. Chem. Soc.* **2010,** *132* (13), 4766–4771.

(9) Gao, Y.; Wang, Z. L. Equilibrium Potential of Free Charge Carriers in a Bent Piezoelectric Semiconductive Nanowire. *Nano Lett.* **2009,** *9* (3), 1103–1110.

(10) Tham, D.; Nam, C. Y.; Fischer, J. E. Defects in GaN Nanowires. *Adv. Funct. Mater.* **2006,** *16*, 1197–1202.

(11) Yamaguchi, M.; Yagi, T.; Sota, T.; Deguchi, T.; Shimada, K.; Nakamura, S. Brillouin scattering study of bulk GaN. *J. Appl. Phys.* **1999,** *85* (12), 8502–8504.

(12) Chen, Y.; Stevenson, I.; Pouy, R.; Wang, L.; McIlroy, D. N.; Pounds, T.; Norton, M. G.; Aston, D. E. Mechanical Elasticity of Vapour-Liquid-Solid Grown GaN Nanowires. *Nanotechnology* **2007,** *18*, 135708.

(13) Ni, H.; Li, X.; Cheng, G.; Klie, R. Elastic modulus of single-crystal GaN nanowires. *J. Mater. Res.* **2006,** *21* (11), 2882–2887.

(14) Henry, T.; Kim, K.; Ren, Z.; Yerino, C.; Han, J.; Tang, H. X. Directed Growth of Horizontally Aligned Gallium Nitride Nanowires for Nanoelectromechanical Resonator Arrays. *Nano Lett.* **2007,** *7* (11), 3315–3319.

(15) Nam, C.-Y.; Jaroenapibal, P.; Tham, D.; Luzzi, D. E.; Evoy, S.; Fischer, J. E. Diameter-dependent Electromechanical Properties of GaN Nanowires. *Nano Lett.* **2006,** *6* (2), 153–158.

(16) Feng, G.; Nix, W. D.; Yoon, Y.; Lee, C. J. A study of the mechanical properties of nanowires using nanoindentation. *J. Appl. Phys.* **2006,** *99* (7), No. 074304-10.

(17) Wang, Z.; Zu, X.; Yang, L.; Gao, F.; Weber, W. J. Molecular dynamics simulation on the buckling behavior of GaN nanowires under uniaxial compression. *Physica E* **2008,** *40* (3), 561–566.

(18) Gulans, A.; Tale, I. Ab initio calculation of wurtzite-type GaN nanowires. *Phys. Status Solidi C* **2007,** *4* (3), 1197–1200.

(19) Vurgaftman, I.; Meyer, J. R. Band parameters for nitrogen-containing semiconductors. *J. Appl. Phys.* **2003,** *94* (6), 3675–3696.

(20) Haque, M. A.; Espinosa, H. D.; Lee, H. J. MEMS for In Situ Testing—Handling, Actuation, Loading, and Displacement Measurements. *MRS Bull.* **2010,** *35* (May), 7.

(21) Park, H. S.; Cai, W.; Espinosa, H. D.; Huang, H. Mechanics of Crystalline Nanowires. *MRS Bull.* **2009,** *34* (March), 7.

(22) Agrawal, R.; Espinosa, H. D. Multiscale experiments - State of the Art and Remaining Challenges. *J. Eng. Mater. Technol.* **2009**, *131*, (4).

(23) Agrawal, R.; Peng, B.; Gdoutos, E. E.; Espinosa, H. D. Elasticity Size Effects in ZnO Nanowires: A Combined Experimental-Computational Approach. *Nano Lett.* **2008,** *8* (11), 3668–3674.

(24) Bertness, K. A.; Roshko, A.; Mansfield, L. M.; Harvey, T. E.; Sanford, N. A. Mechanism for spontaneous growth of GaN nanowires with molecular beam epitaxy. *J. Cryst. Growth* **2008,** *310* (13), 3154–3158.

(25) Bertness, K. A.; Sanford, N. A.; Barker, J. M.; Schlager, J. B.; Roshko, A.; Davydov, A. V.; Levin., I. Catalyst-Free Growth of GaN Nanowires. *J. Electron. Mater.* **2006,** *35* (4), 576–580.

(26) Schlager, J. B.; Bertness, K. A.; Blanchard, P. T.; Robins, L. H.; Roshko, A.; Sanford, N. A. Steady-state and time-resolved photoluminescence from relaxed and strained GaN nanowires grown by catalyst-free molecular-beam epitaxy. *J. Appl. Phys.* **2008,** *103* (124309), 6.

(27) He, M.; Minus, I.; Zhou, P.; Mohammed, S. N.; Halpern, J. B.; Jacobs, R.; Sarney, W. L.; Salamanca-Riba, L.; Vispute, R. D. Growth of large-scale GaN nanowires and tubes by direct reaction of Ga with $NH_3$. *Appl. Phys. Lett.* **2000,** *77* (3731), 3.

(28) Motayed, A.; Davydov, A. V.; Mohammad, S. N.; Melngailis, J. Experimental investigation of electron transport properties of gallium nitride nanowires. *J. Appl. Phys.* **2008,** *104* (024302), 5.

(29) Bertness, K. A.; Roshko, A.; Sanford, N. A.; Barker, J. M.; Davydov, A. V. Spontaneously grown GaN and AlGaN nanowires. *J. Cryst. Growth* **2006,** *287* (2), 522–527.

(30) Zhu, Y.; Espinosa., H. D. An Electromechanical Material Testing System for In situ Electron Microscopy and Applications. *Proc. Natl. Acad. Sci. U.S.A.* **2005,** *102* (41), 14503–14508.

(31) Zhu, Y.; Moldovan, N.; Espinosa., H. D. A Microelectromechanical Load Sensor for In Situ Electron and X-ray Microscopy Tensile Testing of Nanostructures. *Appl. Phys. Lett.* **2005,** *86* (1), No. 013506.
(32) Espinosa, H. D.; Zhu, Y.; Moldovan, N. Design and Operation of a MEMS-Based Material Testing System for Nanomechanical Characterization. *J. Microelectromech. Syst.* **2007,** *16* (5), 1219–1231.
(33) Zhu, Y.; Corigliano, A.; Espinosa, H. D. A Thermal Actuator for Nanoscale In-situ Microscopy Testing: Design and Characterization. *J. Micromech. Microeng.* **2006,** *16*, 242–253.
(34) Agrawal, R.; Peng, B.; Espinosa, H. D. An experimental computational investigation of ZnO nanowires Strength and Fracture. *Nano Lett.* **2009,** *9* (12), 4177–4183.
(35) Egerton, R. F. *Electron Energy-Loss Spectroscopy in the Electron Microscope*; Plenum Press: New York, 1986.
(36) Plimpton, S. J. Fast parallel algorithms for short-range molecular dynamics. *J. Comput. Phys.* **1995,** *117*, 1–19.
(37) http://lammps.sandia.gov/. Accessed September 30, 2010.
(38) Kioseoglou, J.; Polatoglou, H. M.; Lymperakis, L.; Nouet, G.; Komninou, P. A modified empirical potential for energetic calculations of planar defect in GaN. *Comput. Mater. Sci.* **2003,** *27*, 43–49.
(39) Stillinger, F. H.; Weber, T. A. Computer simulation of local order in condensed phases of silicon. *Phys. Rev. B* **1985,** *31* (8), 10.
(40) Soler, J. M.; Artacho, E.; Gale, J. D.; Garcia, A.; Janquera, J.; Ordejon, P.; Sanchez-Portal, D. The SIESTA method for ab initio order-N materials simulation. *J. Physics: Condens. Matter* **2001,** *14*, 2745–2779.
(41) Troullier, N.; Martins, J. L. Efficient pseudopotentials for plane-wave calculations. *Phys. Rev. B* **1991,** *43* (3), 1993–2006.
(42) www.icmab.es/siesta/. Accessed September 30, 2010.
(43) Brown, J. J.; Baca, A. I.; Bertness, K. A.; Dikin, D. A.; Ruoff, R. S.; Bright, V. M. Tensile measurement of single crystal gallium nitride nanowires on MEMS test stages. *Sens. Actuators, A* **2010**; doi:10.1016/j.sna.2010.04.002.
(44) Motayed, A.; Vaudin, M.; Davydov, A. V.; Melngailis, J.; He, M.; Mohammad, S. N. Diameter dependent transport properties of gallium nitride nanowire field effect transistors. *Appl. Phys. Lett.* **2007,** *90* (4), No. 043104-3.
(45) Chen, C. Q.; Shi, Y.; Zhang, Y. S.; Zhu, J.; Yan, Y. J. Size Dependence of Young's Modulus in ZnO Nanowires. *Phys. Rev. Lett.* **2006,** *96*, No. 075505.
(46) Zheng, X.; Zhu, L. Theoretical analysis of electric field effect on Young's modulus of nanowires. *Appl. Phys. Lett.* **2006,** *89* (15), No. 153110-3.
(47) Newnham, R. E. *Structure-Property Relations*; Springer-Verlag: New York, 1975.